

## RESEARCH ARTICLE

10.1002/2016JF004033

## Key Points:

- Results from an extensive new seismic survey of the bed of Pine Island Glacier are presented
- Tributaries of Pine Island Glacier are underlain by widespread low-porosity dilated sediments
- Deep older deposits provide an abundant supply of sediment across the basin

## Correspondence to:

A. M. Brisbourne,  
aleisb@bas.ac.uk

## Citation:

Brisbourne, A. M., A. M. Smith,  
D. G. Vaughan, E. C. King, D. Davies,  
R. G. Bingham, E. C. Smith, I. J. Nias, and  
S. H. R. Rosier (2017), Bed conditions of  
Pine Island Glacier, West Antarctica,  
*J. Geophys. Res. Earth Surf.*, 122, 419–433,  
doi:10.1002/2016JF004033.

Received 21 JUL 2016

Accepted 18 NOV 2016

Accepted article online 22 NOV 2016

Published online 26 JAN 2017

## Bed conditions of Pine Island Glacier, West Antarctica

A. M. Brisbourne<sup>1</sup>, A. M. Smith<sup>1</sup>, D. G. Vaughan<sup>1</sup>, E. C. King<sup>1</sup>, D. Davies<sup>2</sup>, R. G. Bingham<sup>2</sup>, E. C. Smith<sup>1</sup>,  
I. J. Nias<sup>3</sup>, and S. H. R. Rosier<sup>1</sup>
<sup>1</sup>British Antarctic Survey, Natural Environment Research Council, Cambridge, UK, <sup>2</sup>School of GeoSciences, University of  
Edinburgh, Edinburgh, UK, <sup>3</sup>School of Geographical Sciences, University of Bristol, Bristol, UK

**Abstract** Although 90% of Antarctica's discharge occurs via its fast-flowing ice streams, our ability to project future ice sheet response has been limited by poor observational constraints on the ice-bed conditions used in numerical models to determine basal slip. We have helped address this observational deficit by acquiring and analyzing a series of seismic reflection profiles to determine basal conditions beneath the main trunk and tributaries of Pine Island Glacier (PIG), West Antarctica. Seismic profiles indicate large-scale sedimentary deposits. Combined with seismic reflection images, measured acoustic impedance values indicate relatively uniform bed conditions directly beneath the main trunk and tributaries, comprising a widespread reworked sediment layer with a dilated sediment lid of minimum thickness  $1.5 \pm 0.4$  m. Beneath a slow-moving intertributary region, a discrete low-porosity sediment layer of  $7 \pm 3$  m thickness is imaged. Despite considerable basal topography, seismic observations indicate that a till layer at the ice base is ubiquitous beneath PIG, which requires a highly mobile sediment body to maintain an abundant supply. These results are compatible with existing ice sheet models used to invert for basal shear stress: existing basal conditions upstream will not inhibit further rapid retreat of PIG if the high-friction region currently restraining flow, directly upstream of the grounding line, is breached. However, small changes in the pressure regime at the bed, as a result of stress reorganization following retreat, may result in a less-readily deformable bed and conditions which are less likely to maintain high ice-flow rates.

## 1. Introduction

Net mass loss from the Antarctic Ice Sheet is concentrated in the Amundsen Sea Embayment in West Antarctica [Rignot *et al.*, 2011b; Shepherd *et al.*, 2012]. Within this region lies Pine Island Glacier (PIG, Figure 1a), currently the largest single contributor to sea level rise in Antarctica [Shepherd *et al.*, 2012]. Thinning of PIG has been accelerating since the 1980s, and as a result it is currently responsible for 20% of ice discharge from the West Antarctic Ice Sheet (WAIS) and contributes  $\sim 0.12$  mm yr<sup>-1</sup> to sea level rise [Medley *et al.*, 2014; Rignot *et al.*, 2011b; Wingham *et al.*, 2009]. Ice-flow velocity at the grounding line increased by 34% between 1996 and 2006 [Rignot *et al.*, 2008]. Inland thinning rates are an order of magnitude lower than at the grounding line [Wingham *et al.*, 2009] although the response of the tributaries is not uniform [McMillan *et al.*, 2014; Wingham *et al.*, 2009].

The rapid changes in the ice streams of the Amundsen Sea Embayment are widely attributed to oceanographic perturbations. Incursion of relatively warm Circumpolar Deep Water beneath the ice shelves is held responsible for ice shelf thinning through melting of their undersides, in turn reducing the buttressing of upstream grounded ice and facilitating retreat of the grounding line [see Alley *et al.*, 2015, and references therein]. Analysis of a 28 year record of Landsat images by Bindenschadler [2002] indicated that significant migration of the margins in the lower sections of PIG, and ice shelf thinning, was already underway in 1973. Retreat in the early 1970s to behind a submarine sill (Jenkins Ridge) has left the main trunk of PIG resting on a reverse-slope bed [Jenkins *et al.*, 2010]. The stability of this configuration may be critically dependent on buttressing, bedrock topography, and friction at the bed [Nias *et al.*, 2016; Ritz *et al.*, 2015]. Improved constraints on basal properties are therefore imperative to understand the future evolution of PIG. Similarly, the reliability of projections of the future response of PIG is governed in part by a better understanding of the nonuniform behavior of its tributaries. This variation is not simply determined by the gross basal topography; the main trunk of PIG and two of its tributaries lie in deep troughs, whereas ice flow in the remainder of the tributaries is less strongly correlated with bed topography (Figure 1b). As summarized by Peters *et al.* [2006],

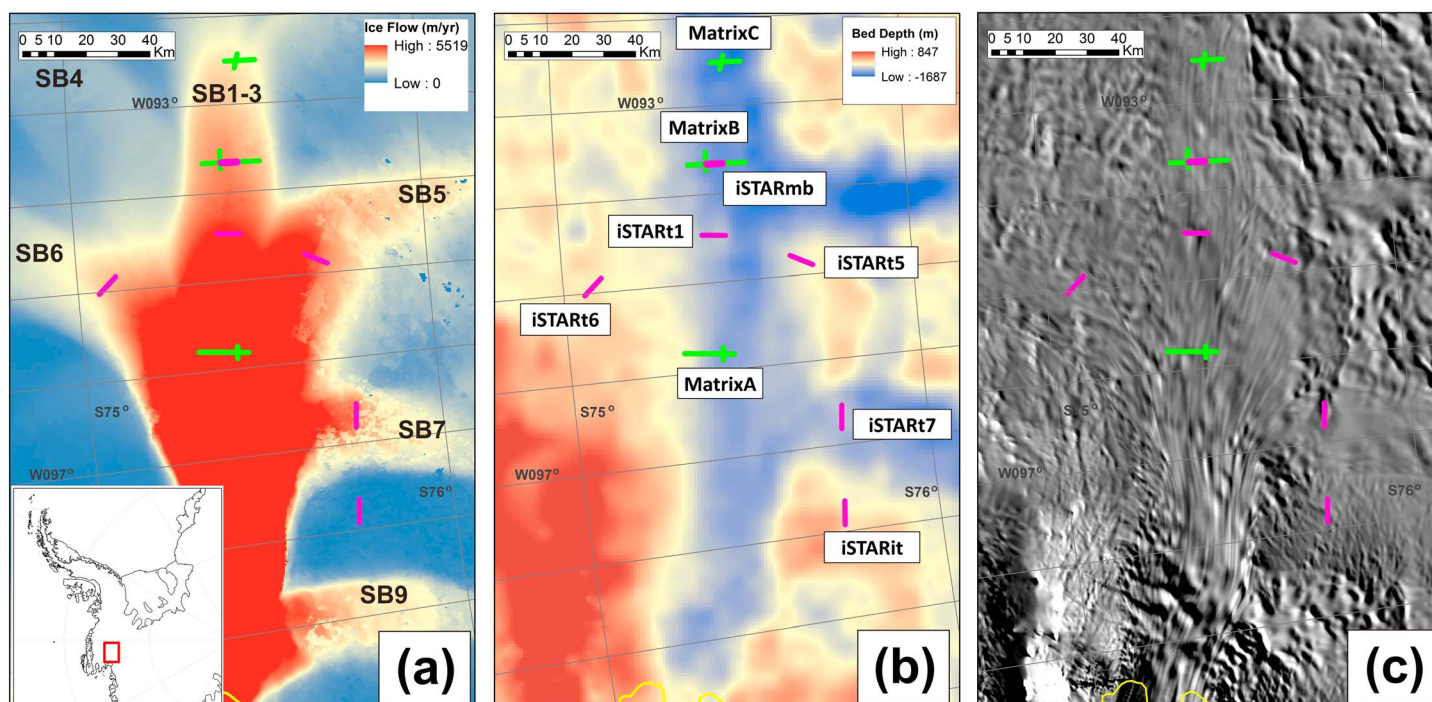


**Figure 1.** Location of seismic profiles across Pine Island Glacier used in this study. The inset in Figure 1a shows the location of the detailed maps of PIG within West Antarctica (red box). (a) Ice-flow speed in  $\text{m yr}^{-1}$  from interferometric synthetic aperture radar (InSAR) measurements [Rignot *et al.*, 2011b]. The “SBx” annotation refers to the tributary nomenclature of Stenoi and Bentley [2000]. (b) Bedmap2 bed elevation [Fretwell *et al.*, 2013]. iSTAR seismic lines (acquired 2014/2015) are in magenta, and Matrix lines (acquired 2006–2008) are in green. (c) Moderate Resolution Imaging Spectroradiometer (MODIS) image [Scambos *et al.*, 2007].

where subdued bed topography exerts less influence on flow, basal conditions, and more specifically the presence, distribution, and water content of subglacial sediments, can have fundamental control over the extent and rate of ice streaming, as exemplified by the Ross Ice Streams across the Siple Coast region of Antarctica [e.g., Blankenship *et al.*, 1986; Engelhardt and Kamb, 1998; Tulaczyk *et al.*, 1998].

Ice sheet models, constrained by satellite and airborne observations, have been used to invert for basal conditions across the entire PIG basin and indicate the presence of a weak sediment beneath the downstream sector and a more “mixed” region of both weak sediment and bedrock further upstream [Joughin *et al.*, 2009]. Smith *et al.* [2013], using both seismic data and airborne potential field data, also inferred the presence of both weak and stiff sediment on the main tributary. Offshore, Pine Island Bay is characterized by regions of thick sediments close to the ice shelf. These sediments become more unevenly distributed farther offshore, resulting in exposed bedrock in places [Muto *et al.*, 2016; Nitsche *et al.*, 2013]. At least part of the region of WAIS currently beneath grounded ice is likely to have been deglaciated in the Pliocene or Pleistocene [Pollard and DeConto, 2009], and as such the presence of considerable amounts of sediments beneath the present-day ice stream is expected. Rippin *et al.* [2011] calculated basal roughness from airborne radar measurements of bed topography. They attribute a smooth bed beneath the main trunk and two tributaries of PIG to the presence of sufficient sediment to allow bed deformation and erosion.

Seismic reflection techniques can be used to distinguish softer deforming sediments from harder nondeforming or consolidated sediments [Smith, 1997a, 1997b, 2007]. Previous results have demonstrated a high degree of variability in basal properties. For example, beneath Rutford Ice Stream, Smith [1997a] discriminated areas of both dilated and lodged till along a seismic line a few kilometers in length. Also in the Weddell Sea region, Vaughan *et al.* [2003] determined a range of basal conditions both across individual ice streams (Rutford and Talutis Inlet) and between adjacent ice streams (Evans and Carlson Inlet). Similarly, inferred till porosity, or till stiffness, varies significantly across Whillans Ice Stream, dependent on the likely hydrological conditions of the area in question, e.g., comparing areas of smooth deformable bed investigated by Blankenship *et al.* [1986] with the “sticky spot” site of Luthra *et al.* [2016].

**Table 1.** Details of the Seismic Profiles Used in This Study

Seismic Experiment	Data Acquisition Field Season	Line Length (Across/Along Flow)	Sensor
MatrixA	2006/2007	16/5 km	100 Hz geophone
MatrixB	2007/2008	18/5 km	100 Hz geophone
MatrixC	2007/2008	10/5 km	100 Hz geophone
iSTAR	2014/2015	5 or 7 n/a	40 Hz georod

In this study we present results from a series of seismic reflection lines across PIG. Seismic imaging and the strength of reflections from the ice stream bed are here used to constrain subglacial bed properties. Seismic results are consistent with a widespread dilated sediment layer at the bed which would enable rapid ice flow. We demonstrate the presence of this readily deformable layer, even over topographic highs, where the scouring of any sediment to expose the more flow-resistant bedrock may have been expected. In contrast, the bed beneath an intertributary area of slow-moving ice is shown to be underlain by much lower porosity or frozen sediments. We show that these results corroborate previous studies which used remotely sensed observations to infer basal shear stress.

## 2. Data and Methods

The data used for this study consist of a series of seismic reflection profiles acquired across PIG and its tributaries over three field seasons (Figure 1). Profiles acquired in 2006/2007 and August 2007/2008 are collectively termed “Matrix”; profiles acquired in austral summer 2014/2015 are labeled “iSTAR”. Where necessary, we have assigned individual seismic profile names following the tributary nomenclature of *Stenoien and Bentley* [2000] (see Table 1 and Figure 1a). Although acquired over three different field seasons, the field methods were consistent throughout each of the field campaigns and all data were processed in a similar manner to maintain consistency. Any differences are specified in the text below.

### 2.1. Data Acquisition

The seismic source used for the reflection profiles was 300 g of high explosive, placed in holes of 20 m depth, backfilled with snow. A shot interval of 240 m and receiver interval of 10 m with 30 m offset was used throughout to produce single-fold normal-incidence ( $<10^\circ$  incidence angle) data with a midpoint interval of 5 m. A 48 channel Geode seismic system recorded 2 s record lengths at 8000 Hz sample rate. The only marked difference in acquisition hardware between seasons was the use of 100 Hz geophones on the Matrix lines and 40 Hz georods [Voigt *et al.*, 2013] on the iSTAR lines, which demonstrably improves the signal to noise ratio. The method of determining the absolute reflection coefficient of the bed relies on the calibration of the primary bed reflection with a coincident multiple reflection [see Roethlisberger, 1972; Smith, 1997a; Holland and Anandakrishnan, 2009]. Where multiple bed returns are not available on the primary seismic reflection line data, larger shots were used with a longer record length to capture the multiple.

#### 2.1.1. iSTAR Seismic Data

Locations for seismic profiling in 2014/2015 were identified using radar data that were acquired at each of the sites in the previous season. The radar data were acquired in a series of  $15 \times 10$  km “patches” wherein radar processing revealed the presence of a range of subglacial regimes and bedforms underlying the ice at each of the survey sites [Bingham *et al.*, 2014]. Seismic reflection profiles 7.2 km in length were acquired at each site, with the specific selection of profiles at each site designed overall to sample a range of bed features characteristic of the entire basin. With the exception of line iSTARit, which is on a slow-moving intertributary bed elevation high, all iSTAR seismic lines were acquired on fast-flowing tributaries. All iSTAR lines were acquired “across flow,” i.e., orthogonal to the overall ice-flow direction, with the aim of sampling a wider range of bed conditions than would likely be achieved along flow due to the linear nature of the bed forms along flow.

#### 2.1.2. Matrix Seismic Data

The Matrix lines, acquired in 2006/2007 and 2007/2008, were located on the main trunk of PIG and farther up the main tributary (Figure 1b). Long lines were acquired across ice flow, and intersecting shorter lines were acquired along flow (Table 1). One additional seismic line was acquired in 2014/2015, iSTARmb, and is a repeat survey of a 5 km section of the MatrixB line (Figure 1b).

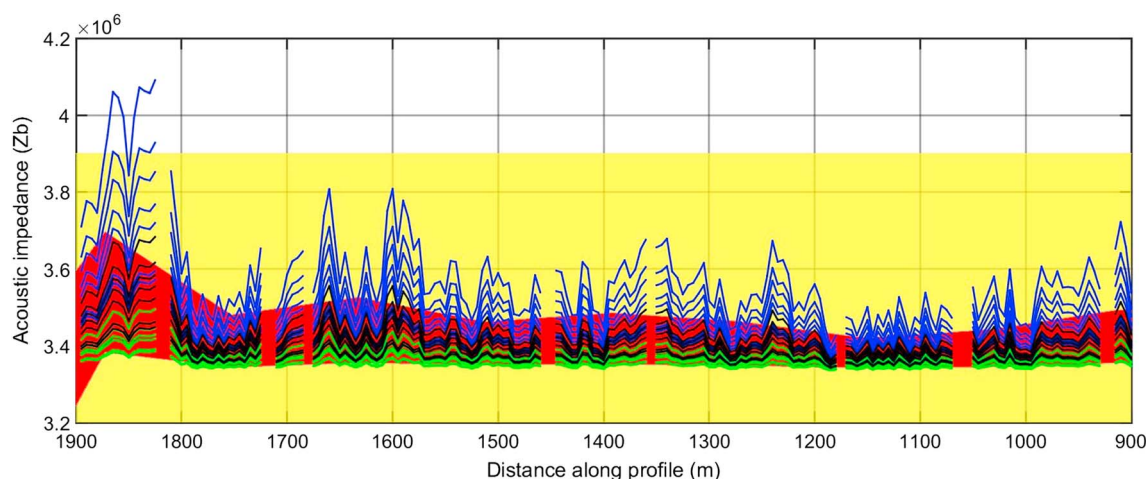


**Figure 2.** Raw bed acoustic impedance values in  $\text{kg m}^{-2} \text{s}^{-1}$  over a 1 km section of iSTART7 demonstrating the spatial variability of raw data and the smoothing effects of binning. Colored lines represent acoustic impedance values calculated using all applicable multiple reflections for this seismic profile: black lines, assumed parameters; green lines, minimum possible values calculated with measurement and assumed parameter uncertainties; and blue lines, maximum possible values calculated with uncertainties. The red band is the first standard deviation of the binned values of the acoustic impedance as described in the text. The yellow band indicates the likely acoustic impedance values of diluted sediments generally associated with the deformation of bed material [Aire and Bentley, 1993]. The ice-flow direction is into the page.

## 2.2. Data Processing and Calculation of Bed Acoustic Impedance

The absolute reflection coefficient of the bed was determined following the method of Smith [1997a], using the ratio of the energy of the primary and multiple bed reflections. This method requires reliable amplitude recovery from the data. As such, data processing is kept to a minimum, with only normal moveout and static corrections being applied prior to time domain migration. Ice thickness is determined from seismic travel-times, corrected for the reduced velocity in the firn which is derived from shallow seismic refraction experiments [Kirchner and Bentley, 1990]. Seismic attenuation in the ice of  $2 \pm 1 \times 10^{-4} \text{ m}^{-1}$  is assumed, based on the likely temperature profile of the ice column [Bentley and Kohnen, 1976]. Derivation of the acoustic impedance of the bed material from the calibrated reflection coefficient requires the acoustic impedance of the basal ice to be assumed. A value of  $3.33 \pm 0.04 \times 10^6 \text{ kg m}^{-2} \text{s}^{-1}$  is used here, based on the likely basal-ice conditions [Aire and Bentley, 1993]. From the calculated acoustic impedance measurements of the base, inferences about likely bed materials can be drawn and are discussed below.

Bed picks are made at the first-arriving energy of the primary and multiple bed reflections in the seismic section and 5 ms time windows exported to encapsulate the Ricker wavelet of the first arrival. The sum of the square of the amplitudes is then used to determine the energy of the ice-base reflection and multiple. A calibrated bed reflection coefficient can be determined at the site of the bed multiple and then extrapolated along the entire line using the energy of the primary bed reflection. Unlike previous studies, e.g., Smith *et al.* [2013], where a single multiple reflection per line has been used, the calculations are carried out separately for every applicable multiple recorded, allowing verification of the result and quantification of the uncertainty resulting from shot-to-shot variability and any lateral variation in ice properties.

## 2.3. Uncertainties in Acoustic Impedance Measurements

For each trace along the seismic line where a bed pick can be made, the measured, minimum, and maximum acoustic impedance values are calculated, determined using the uncertainties in the measurements and assumed parameters as described above. The calculation is repeated at each bed pick for every multiple applicable to that line to produce a population range including all likely maximum and minimum acoustic impedance values. This population is then used to determine the standard deviation of possible measured values at each point to describe the likely range of values. Measured acoustic impedance values and uncertainties are then averaged over 24 channels, or 120 m bed interval bins, equivalent to the first Fresnel zone of the unmigrated data (150 Hz center frequency and 1600 m depth). This averaging reduces the effects of laterally varying thin bed layers, migration artifacts, and non-2D structure, and also indicates variance in the observations allowing quantification of the uncertainty. Figure 2 demonstrates the effect of uncertainties



and smoothing along a 1 km section of iSTART7. Black lines represent the raw acoustic impedance values calculated using measured amplitude values and assumed parameters without uncertainties. The green and blue lines represent the minimum and maximum raw acoustic impedance values calculated using uncertainties. The nonlinear effect of the uncertainties is demonstrated by the increased spread of measurements away from the reference acoustic impedance value of ice ( $3.33 \times 10^6 \text{ kg m}^{-2} \text{ s}^{-1}$ ) and also in the asymmetry of the first standard deviation of the measurement population.

For lines where no multiple bed returns were recorded, data from adjacent lines are used to calibrate the reflection coefficient. Consistency in acquisition procedures and an assumption of laterally consistent ice properties are required for this step. Testing this assumption is possible on a line where multiples are available, such as iSTART5: the mean difference in basal acoustic impedance along this line between the analysis using multiples from iSTART5 itself and that using multiples from the adjacent iSTART7 line is <1%. This indicates good consistency in the acquisition procedures and little lateral variation in ice properties.

Seismic attenuation in ice is controlled primarily by ice temperature [Peters *et al.*, 2012, and references therein]. Therefore, the attenuation coefficient value used is based on previous studies in regions with a similar temperature range [Smith *et al.*, 2013]. Uncertainties in seismic attenuation of  $1 \times 10^{-4} \text{ m}^{-1}$  encapsulate the likely temperature range and uncertainty in previous attenuation measurements and are included in the variance of the final acoustic impedance observations presented here. Where multiples from adjacent lines are used to calibrate the reflection coefficient, the range of possible seismic attenuation values is doubled to accommodate variation in the ice column due to advection from different locations. We attempted to minimize shot-to-shot variability at the data acquisition stage by ensuring a consistent field methodology to achieve uniform shot and receiver coupling. The most difficult aspect of the field acquisition to repeat uniformly is the backfilling of shot holes: A funnel with a coarse grating was therefore placed over the shot hole and only cold and dry snow used. However, shot-to-shot variation in the amplitude of direct-path energy is still observed, indicative of a variation in source amplitude, assuming that variation in seismic attenuation is negligible over distances of a few hundred meters [Holland and Anandakrishnan, 2009]. We therefore correct for variability in shot coupling by quantifying the energy in the ground roll or direct-wave surface noise. Shot gathers are normalized for shot-to-shot variability according to the energy recorded at each receiver during a 200 ms window of data following the first arrival. In most cases, the correction for shot-to-shot variability has little effect on the acoustic impedance results. However, data from MatrixB show appreciable shot-to-shot variation in the ground roll energy, such that the correction cannot be applied without skewing the data beyond physically realistic limits. Though we do not know the exact cause of this, we note that the ice at MatrixB was under extremely high tension during the period of seismic-data acquisition [Scott *et al.*, 2010], and we hypothesize that microfractures may have been present beneath the surface which would have affected the lateral propagation of seismic energy. As such, no shot-to-shot correction is made. The results for MatrixB are therefore regarded as less-well constrained than the other lines. However, as the seismic energy of the bed reflections is vertically propagating, the impact of surface cracks on the bed reflections is less significant than on the ground roll, and it is likely that the MatrixB data are comparable to the other lines.

The effect of the change in hardware from 100 Hz geophones on the Matrix lines to 40 Hz georods on the iSTAR lines was tested. To emulate the geophone data of the Matrix lines, a 100 Hz high-pass filter was applied to the raw seismic data from line iSTART6, where the highest number of coincident multiple reflections for calibration was observed. The mean difference in the calculated acoustic impedance results between the filtered and unfiltered data is less than 0.3% and therefore deemed negligible.

### 3. Seismic Observations and Interpretation

#### 3.1. Seismic Profiles

The large range of bed topography across the tributaries is indicated by an obvious ice-base reflection in all seismic sections and is in agreement with coincident radar-derived bed topography [Bingham *et al.*, 2014], with changes of a few hundred meters vertically over a few kilometers laterally on a number of profiles. Example seismic sections illustrating key features are presented in Figure 3. Seismic reflections consistent with deeper sedimentary layering are observed at up to 100 ms two-way traveltime beneath the ice-bed interface at a number of sites, e.g., iSTART1 (Figure 3a) and iSTART5 (Figure 3b). The sedimentary structures

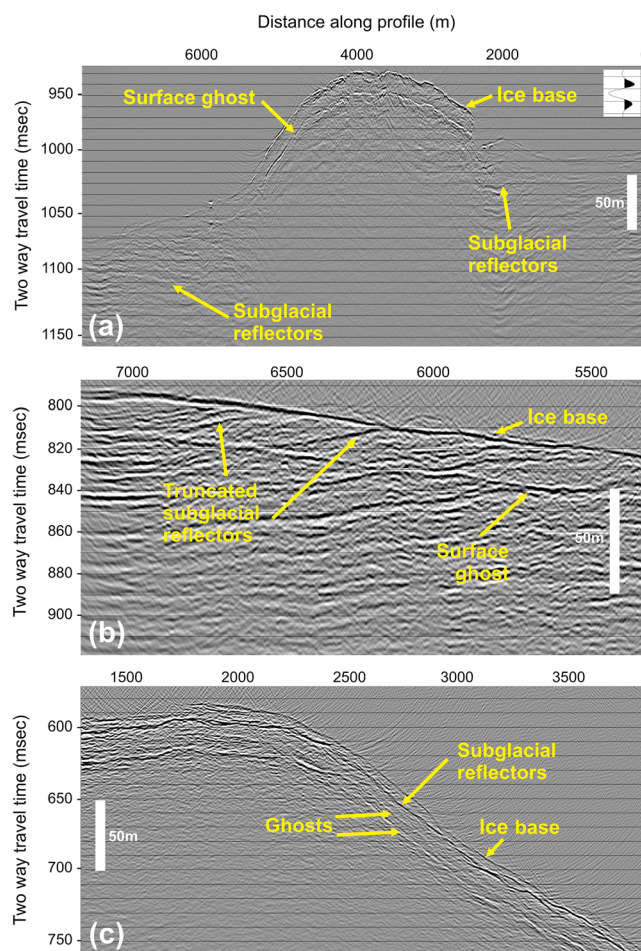


**Figure 3.** Example of migrated seismic sections (a) iSTARt1: a clear ice-base reflector is observed along the entire profile beneath  $>1600$  m of ice. Sub-bed reflectors are visible at the margins of the topographic high only. Inset: An example of Ricker wavelet from a relatively low acoustic impedance subglacial bed (i.e., high-porosity dilated sediment) to highlight the polarity convention; (b) iSTARt5: illustrating details of stratigraphic structure beneath the ice-bed interface of a tributary. Reflectors within the bed are truncated by a thin layer at the interface but maintain coherency close to the interface; (c) iSTARit: illustrating details of stratigraphic structure beneath the ice of the intertributary profile. Vertical scale bars represent thickness beneath the ice base assuming a  $P$  wave velocity in sediment of  $2000 \text{ m s}^{-1}$ . Distance along profile values refers directly to Figure 4a. The ice-flow direction is into the page.

imaged in the seismic profiles, such as dipping reflectors truncated by the ice base, indicate that these are older sediments which must predate the current glacial cycle. Assuming a typical seismic velocity in consolidated sediments of  $2000 \text{ m s}^{-1}$  [Smith *et al.*, 2013], these observations are consistent with  $>100$  m thick sedimentary sequences, indicating deep sedimentary deposits immediately beneath the ice base. In general, we do not observe these preexisting sedimentary features beneath topographic highs of the bed. Along profile iSTARit, between tributaries, we observe continuous seismic reflections almost parallel to the bed, consistent with a discernible basal sediment layer of variable thickness (Figure 3c). Similar but less continuous reflections are observed along short sections of profiles iSTARt1 and iSTARt7.

With the exception of iSTARit, and possibly short sections of the Matrix profiles, the bed reflections on all the seismic lines are either negative or weak and positive. The polarity of the bed reflection is in itself diagnostic [Atré and Bentley, 1993]; the acoustic impedance of ice is very similar to that of dilated sediment, and therefore, a small change in the acoustic impedance across this threshold results in a polarity change of the bed reflection which is observed: Rapid reversals in polarity may indicate a basal acoustic impedance value close to that of ice with only slight variation. A negative reflection coefficient can be unambiguously interpreted as high-porosity sediment or water: a positive reflection coefficient is more ambiguous, indicating high-porosity sediment

if the reflection is weak, or else harder material if the reflection is strong. Where the reflection is very weak the polarity becomes harder to discriminate unambiguously. However, as the acoustic impedance value remains close to that of ice the interpretation is still valid.

### 3.2. Acoustic Impedance of the Bed Material

The acoustic impedance measurements of the bed along all seismic profiles are shown in Figures 4a and 4b, with the uncertainty to one standard deviation plotted. Likely basal materials can be determined by comparison of measured acoustic impedance values with those typical of dilated sediment, stiff sediment, or lithified sediment, a frozen bed or crystalline bedrock [Smith, 1997a]. For reference, the acoustic impedance values of water and basal ice are plotted. The yellow band highlights the approximate range of acoustic impedance values expected for a dilated sediment associated with bed deformation, which would exhibit a porosity in

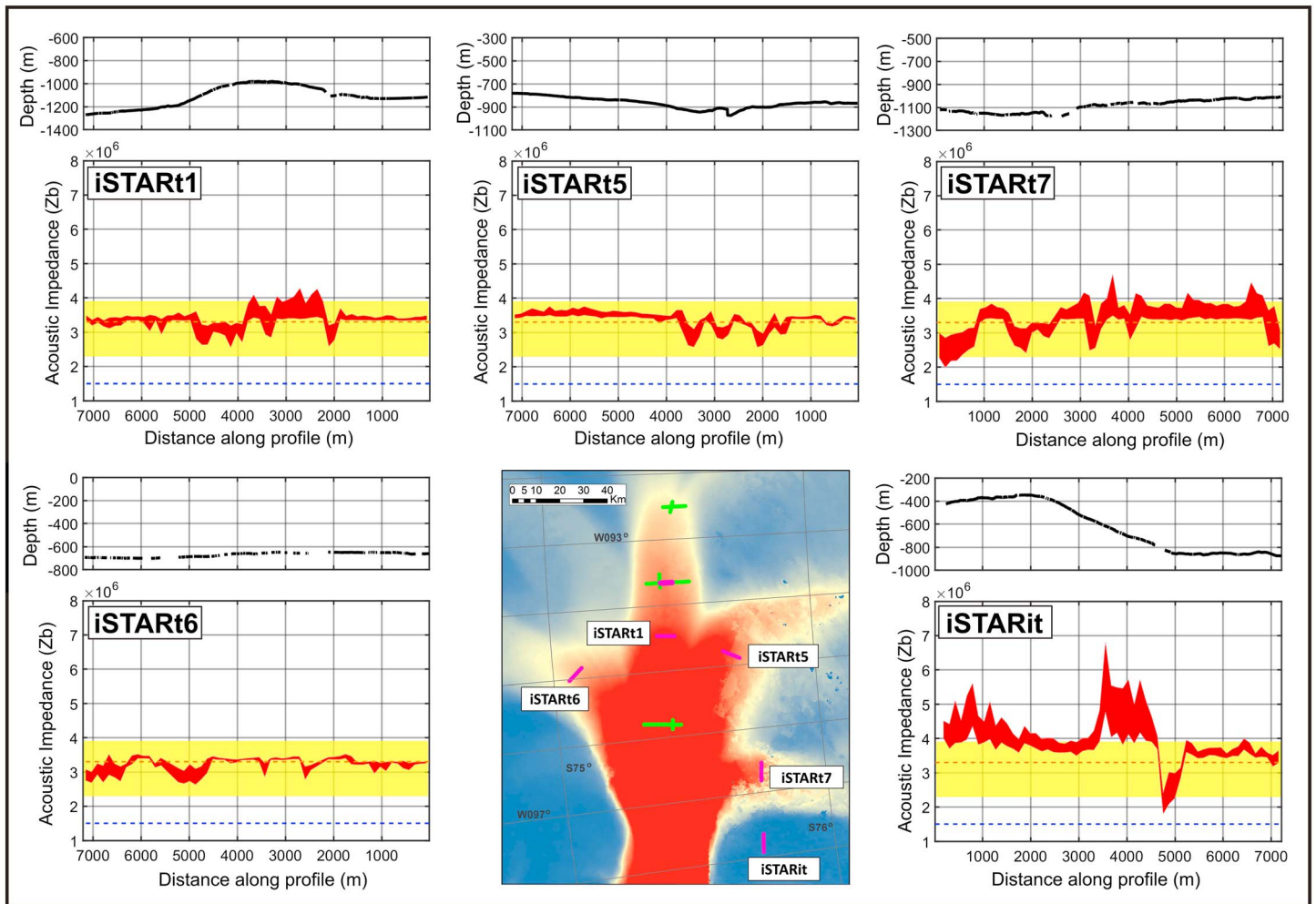


**Figure 4a.** Bed elevation in meters (upper plots) and bed acoustic impedance in  $\text{kg m}^{-2} \text{s}^{-1}$  (lower plots) measured along iSTAR seismic profiles. The blue dashed line indicates the acoustic impedance value of water; the brown dashed line indicates the acoustic impedance value of ice; the yellow band indicates the likely acoustic impedance values of dilated sediments generally associated with the deformation of bed material [Aire and Bentley, 1993]. The ice-flow direction is into the page.

the range of 30–45% [Aire and Bentley, 1993]. Acoustic impedance values above this range are consistent with a lodged till with porosity  $\leq 30\%$ , poorly lithified sedimentary rock, or, at even higher values, a frozen bed [Smith, 1997a].

Across all surveyed tributaries, the mean acoustic impedance value of the bed immediately beneath the ice base is  $3.0 \pm 0.2 \times 10^6 \text{ kg m}^{-2} \text{s}^{-1}$ , consistent with a dilated sediment of 35–45% porosity [Aire and Bentley, 1993]. In contrast, the mean acoustic impedance along profile iSTARit, between tributaries, is  $3.9 \pm 0.3 \times 10^6 \text{ kg m}^{-2} \text{s}^{-1}$ , consistent with stiffer lower porosity sediment, increasing to a mean of  $4.7 \pm 0.6 \times 10^6 \text{ kg m}^{-2} \text{s}^{-1}$  along the middle section of the line.

The most striking feature of the acoustic impedance results is their consistency across a range of basal topography. The Matrix lines (located along the central trunk and upstream main tributary) indicate a greater variation than the iSTAR lines (more widely spread around the basin), but this also encompasses a greater uncertainty in the results, most likely due to the use of geophones rather than georods [Voigt et al., 2013], as well as the surface fractures noted at MatrixB. This is evident in the iSTARmb data which are coincident with the MatrixB results. The iSTARmb line is a repeat of a section of the MatrixB line (Figures 1b and 4b) and would therefore be expected to reproduce the earlier results with any temporal changes superimposed. Although the results are consistent, the significantly higher uncertainties assigned to the



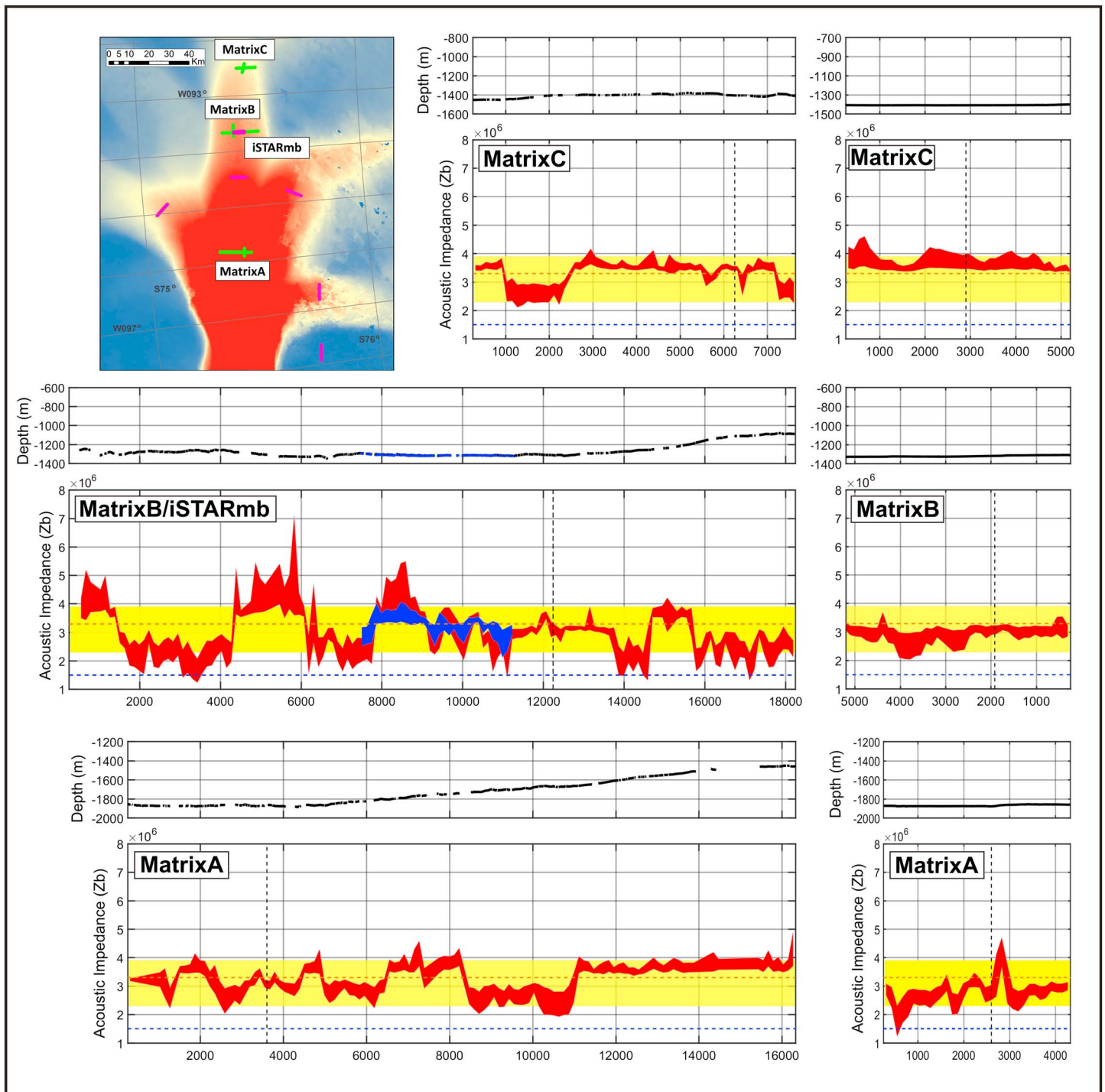


**Figure 4b.** Bed elevation in meters (upper plots) and bed acoustic impedance in  $\text{kg m}^{-2} \text{s}^{-1}$  (lower plots) measured along Matrix seismic profiles as per Figure 4a. Across-flow profiles are to the left, along-flow plots are to the right. The crossing locations of the Matrix along- and across-flow lines are highlighted with the black dashed line. iSTARmb results are overlain in blue on the MatrixB results. iSTARmb results are consistent with the MatrixB results within uncertainties but highlight the lower uncertainties in the more recent data acquisition. The ice-flow direction is into the page across flow and left to right along flow.

MatrixB data are clearly demonstrated. An earlier analysis of the MatrixB data by *Smith et al.* [2013] interpreted a basal sediment layer with lateral variation between soft and hard sediment. However, the more recent iSTARmb data, with lower uncertainties, and the higher uncertainties assigned here to the earlier MatrixB data, preclude such an interpretation along the repeated sections of seismic lines and



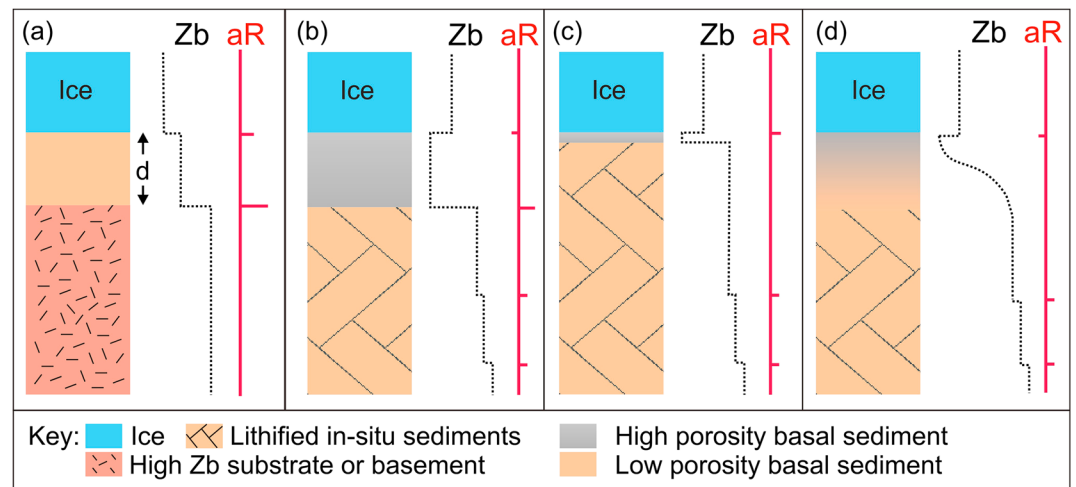


**Figure 5.** Schematic of possible basal structures directly beneath the ice with respective acoustic impedance values (Zb) and apparent reflection coefficients (aR). (a) The likely conditions beneath the intertributary line and (b–d) likely conditions beneath the tributaries. Thick ( $d > \lambda/4$ ) low-porosity basal sediment layer directly overlying a substrate of different lithology (Figure 5a); thick ( $d > \lambda/4$ ) high-porosity basal sediment layer over in situ sediments with sharp acoustic impedance contrast (Figure 5b); thin ( $d < \lambda/4$ ) high-porosity basal sediment layer over in situ sediments with sharp acoustic impedance contrast resulting in a reverse polarity in the apparent reflectivity (Figure 5c); and thick ( $d > \lambda/4$ ) reworked basal sediment layer with acoustic impedance gradient to deeper sediment, resulting in a weak negative reflection coefficient at the ice base (Figure 5d).

therefore reduce confidence in the MatrixB data elsewhere. Segments of the intertributary line, with acoustic impedance measurements above that of dilated sediments, are the only indication of either a stiff low-porosity sediment or frozen bed. These results are consistent with inferred basal temperature models [Joughin *et al.*, 2009].

### 3.3. Constraining the Nature and Thickness of the Basal Sediment Layers

We constrain basal sediment layer thickness by combining seismic imaging, measured acoustic impedance values, and assumed seismic velocity values from previous studies appropriate to the measured acoustic impedance contrast at the ice base.

#### 3.3.1. Constraining the Thickness of the Intertributary Basal Layer

Along profile iSTARit, acquired on slow-moving ice between tributaries 7 and 9, a clear reflection is observed directly after the ice-base reflection (Figure 3c), indicating a discrete subglacial sediment layer (Figure 5a). The layer thickness varies laterally. The strong positive reflection from the base of this layer indicates a substrate of relatively high acoustic impedance directly beneath the ice. Similar reflectors are reported elsewhere [e.g., Horgan *et al.*, 2013; Luthra *et al.*, 2016; Rooney *et al.*, 1987] and associated with a deforming sediment layer. Where a clear reflection from the base of the subglacial layer is recorded we can estimate layer thickness directly. Assuming a seismic velocity in this layer of  $2120 \pm 200 \text{ m s}^{-1}$  [Luthra *et al.*, 2016], consistent with the positive ice-base reflection coefficient and relatively high acoustic impedance substrate compared to the tributaries, we can constrain the mean thickness to  $7 \pm 3 \text{ m}$  with a maximum thickness of 13 m. The highest acoustic impedance values at the ice base are observed along the intertributary line iSTARit and are coincident with the absence of the basal sediment layer and may represent the in situ material. In general, beneath sections of the profiles where clear reflections from basal layers are present, no sedimentary features are observed. We therefore infer that this layer at the ice base is a discrete sediment layer overlying a substrate of different lithology (Figure 5a). Although the layer thickness is similar to that observed beneath Whillans Ice Stream [Rooney *et al.*, 1987], the acoustic impedance measurements do not infer an actively deforming layer beneath the intertributary ice. The origin of the layer may be similar, perhaps having formed previously during a period of faster ice flow, but now likely represents a stiff nondeforming till.

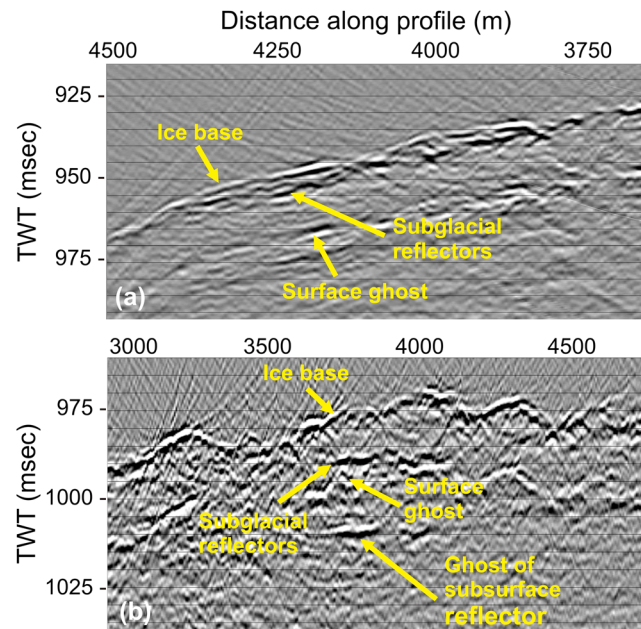


**Figure 6.** Details of migrated seismic sections highlighting the discontinuous seismic reflectors directly beneath the ice base of the tributaries (a) iSTART1 and (b) iSTART7. Distance along profile values refer directly to Figure 4a. The ice-flow direction is into the page.

### 3.3.2. Constraining the Nature of the Basal Layer Beneath the Tributaries

In contrast to the intertributary measurements, the acoustic impedance measurements along the fast-flowing tributaries indicate high-porosity dilated sediments at the ice base, with either a negative or weak-positive ice-base reflection, consistent with a subglacial till [Blankenship *et al.*, 1986; Engelhardt and Kamb, 1998; Tulaczyk *et al.*, 2000a]. The presence of deeper reflectors in the seismic sections confirms that sufficient energy is propagating beneath the ice base reflector to allow discrimination of the base of the till layer if sufficiently thick and of sufficiently high acoustic impedance contrast to its substrate (Figure 5b). However, the seismic profiles along the tributaries do not indicate extensive, consistent, or unambiguous bed-parallel reflections as observed on the intertributary profile. The absence of bed-parallel reflections does not preclude the pre-

presence of a basal till layer: the till layer may be too thin to be resolved by the seismic wavelength of our data (Figure 5c), in which case the reflections from the upper and lower interfaces of the till layer form a composite wavelet [Booth *et al.*, 2012], resulting in an apparent acoustic impedance contrast (aR) which may not be representative; or the lower boundary of the basal layer may be seismically transparent due to an acoustic impedance gradient rather than a sharp contrast at its base (Figure 5d), indicative of a reworked sediment layer.

In the absence of a till-base reflection we can infer the likely thickness range of the layer by assuming ranges of acoustic impedance values consistent with previous studies [Aire and Bentley, 1993]. Observations of preexisting sedimentary stratigraphy beneath the till layer (Figure 3b) are consistent with a more consolidated or lithified substrate, implying material with an acoustic impedance of  $5.5 \pm 1.0 \times 10^6 \text{ kg m}^{-2} \text{ s}^{-1}$  [Smith *et al.*, 2013].

### 3.3.3. Constraining the Thickness of the Basal Layer Beneath the Tributaries

As stated above, in general, no seismic reflection is visible from the base of the high-porosity sediment layer at the bed of the fast-flowing tributaries. However, this dilated lid must be of sufficient thickness to result in a negative reflection coefficient measurement, as observed along large segments of the profiles. Below a layer thickness of  $\lambda/4$  (one quarter of the seismic wavelength in the layer), the reflection coefficient becomes a composite of the upper and lower boundaries, the negative polarity of the reflection becomes increasingly difficult to identify above the background noise, and the apparent reflection coefficient switches polarity to reflect the higher acoustic impedance sediments imaged directly beneath. We therefore use this limit to assign a minimum lid thickness of  $1.5 \pm 0.4 \text{ m}$ , constrained by the measured maximum peak frequency of  $260 \text{ Hz}$  and seismic velocity in the high porosity till of  $1600 \pm 100 \text{ m s}^{-1}$  [Blankenship *et al.*, 1986]. To account for the likely presence of an acoustic impedance gradient beneath this layer, rather than a sharp impedance contrast, we assign a large uncertainty.

The absence of a continuous seismic reflection from the base of this layer beneath the tributaries prevents direct measurement of maximum layer thickness except in a few localized sections of profiles iSTART1 and iSTART7 (Figure 6), where a layer thickness range of 6 to 10 m is calculated assuming a high-porosity till velocity of  $1600 \pm 100 \text{ m s}^{-1}$ , compatible with the negative reflection coefficient at the ice base [Blankenship *et al.*, 1986]. Also, where we observe the truncation of dipping reflectors (e.g., iSTART5; Figure 3b) we can infer that

the thickness of the reworked layer may be as low as the tuning thickness of the layer, equivalent to one quarter of a wavelength, or  $\sim 2$  m (assuming  $1600 \text{ m s}^{-1}$  for high-porosity sediment). We therefore do not assign a maximum thickness to the reworked sediment layer other than to state that it is laterally variable, and the thickness has been measured at up to 6 to 10 m.

The absence of a basal reflection from a layer greater than the tuning thickness, as is likely to be the case here between the derived end-member thickness measurements, requires that the increase in acoustic impedance with depth within this layer must be gradational, from that of high porosity sediment at the top to more consolidated sediments at the base. This interpretation is consistent with a layer formed by the reworking of existing sediments, as outlined in Figure 5d.

Our preferred model therefore consists of an upper layer of dilated till with minimum thickness  $1.5 \pm 0.4$  m immediately at the ice base, which forms the lid of a reworked sediment layer of variable thickness. Where a positive reflection coefficient is measured, this dilated lid layer must be too thin to be resolved or at the lower end of the proposed porosity range, but always distinct from the deeper sediments with a higher acoustic impedance. We summarize the likely basal conditions in the tributaries in Figure 5.

#### 4. Discussion

Across both the main trunk of PIG and all surveyed tributaries acoustic impedance results indicate widespread dilated sediment of relatively high porosity (30–45%) at the ice base. This layer is most likely formed of reworked sediments and includes a high-porosity lid of minimum thickness  $1.5 \pm 0.4$  m. The thickness of the reworked layer is, in general, poorly constrained due to the seismically transparent base or thin nature, although in places is measured at 6 to 10 m. Although such high-porosity sediment is generally associated with active deformation [Alley *et al.*, 1987], the resolution of the seismic data does not allow us to discriminate whether deformation of the basal till is by deep ploughing [Brown *et al.*, 1987], sliding on discrete planes, or pervasive with depth within the layer. The dilated sediment lid thickness estimated here is greater than the few decimeters of actively deforming till layers observed on glaciers flowing at more moderate rates [Cuffey and Paterson, 2010, Table 7.4, and references therein]. It is possible that deformation is localized to the top of the sediment, and this layer allows pathways for water drainage at the interface with the thawed bed, as observed on the Siple Coast of the WAIS [Kamb, 2001]. Although sparse, these thickness estimates are comparable to the 6–8 m till layer observed beneath Whillans Ice Stream [Blankenship *et al.*, 1987; Luthra *et al.*, 2016; Rooney *et al.*, 1987], which flows at a similar rate to the tributaries of PIG. Again, in a similar manner, the actively deforming till layer beneath Whillans Ice Stream unconformably overlies older sedimentary rocks [Luthra *et al.*, 2016].

Beneath slow-moving ice, between tributaries, a well-defined basal sediment layer of thickness  $7 \pm 3$  m is observed. Acoustic impedance measurements indicate lower porosities than those observed beneath the fast-flowing tributaries, with the basal layer overlying material of higher acoustic impedance. Seismic reflections are not observed beneath this layer and may therefore indicate massive homogeneous sediment or a crystalline basement.

The seismic observations indicate widespread sediments, and as such imply that the system is not supply limited and likely to be in a steady state rather than transitional. This conclusion is supported by the presence of deep sequences of older sediment in the seismic profiles. However, the high-porosity sediment cover is thin in places, e.g., iSTART5 between 6000 and 6500 m (Figure 3b), indicating a complex regime of erosion, transport, and deposition controlled by bed geometry, the stress regime in the ice and sediment rheology. Scouring of subglacial sediment at prominent topographic features would generally be expected across the highly variable basal topography of the surveyed sites [Nitsche *et al.*, 2013]. Both Lowe and Anderson [2003] and Nitsche *et al.* [2013] describe a range of seabed morphologies offshore of PIG, from thin or absent sediment cover and exposed bedrock in the central region to thick sedimentary strata immediately offshore of the ice shelf. The results of Muto *et al.* [2016], from the inversion of airborne gravity data, indicate an 800 m deep sedimentary basin immediately offshore of the grounding line of PIG with either thin sediment cover or exposed crystalline basement beyond the Jenkins Ridge. These offshore observations are consistent with the likely onshore subglacial regimes presented here: widespread sediment cover is viable due to an abundant supply from older sedimentary sequences; topographic highs at the bed are a result of more resistant



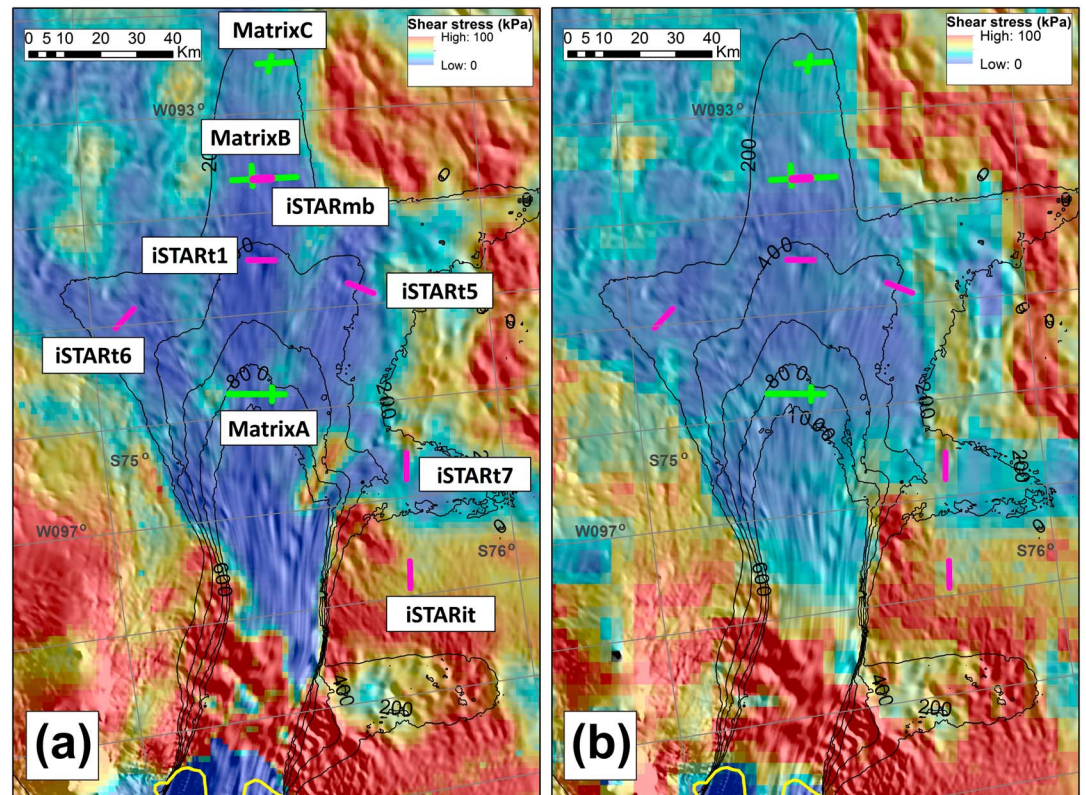


**Figure 7.** Location of seismic profiles (iSTAR, magenta; Matrix, green) with respect to basal shear stress derived from ice sheet models: (a) *Joughin et al.* [2009] and (b) *Arthern et al.* [2015]. Ice flow speed from Differential InSAR [*Rignot et al.*, 2011b] is contoured from 200 to 1000  $\text{m yr}^{-1}$  at 200  $\text{m yr}^{-1}$  intervals. The grounding line in 1999/2000 from MEaSUREs [*Rignot et al.*, 2011a, 2011b] is represented by the yellow line. The MODIS Mosaic [*Scambos et al.*, 2007] showing mean surface morphology is underlain.

lithologies, possibly massive sediments or crystalline basement, with a widespread but thin sediment cover; and a temperature-pressure regime exists beneath the tributaries which ensures bed materials remain unfrozen and deformable or mobile.

The seismic observations presented here constrain basal conditions at a scale which is significantly smaller than those previously inferred with numerical basal shear inversions. Likewise, the comparison of observational results at the small scale with models at a large scale does not provide validation. However, with the ultimate aim in mind of using field-based geophysical observations to constrain large-scale numerical inversions it is useful to compare the broader patterns of the relatively small-scale features determined here with the basin-scale features derived from satellite observations and numerical inversions. *Joughin et al.* [2009] used ice velocity, surface elevation, and bed elevation data to derive basal conditions of PIG and Thwaites Glacier. Although they find strong basal melting in areas upstream of the grounding line, farther inland a “mixed” bed is inferred, with extensive areas of both bedrock and weak sediment. This observation is not consistent with the results presented. Our observations are dominated by the widespread dilated sediment at the ice base. However, projection of the locations of the seismic lines on to these basal shear stress results (Figure 7a) indicates that the seismic profile locations map to areas of relatively low basal shear stress, consistent with the sediment drape results presented here. Similar conclusions can be drawn by comparison to the results of *Arthern et al.* [2015] in Figure 7b. Both of these models indicate a region of higher friction immediately upstream of the grounding line which is currently preventing further rapid retreat of PIG to the upstream region where low basal stress is currently exhibited and areas of low topographic restraint exist [*Joughin et al.*, 2009].

Similarly, *Smith et al.* [2013] presented the data from MatrixB, alongside airborne potential field data, and interpreted the lateral variation in acoustic impedance as being consistent with the results of *Joughin et al.* [2009].

The uncertainties allocated here to the MatrixB data are higher than those assigned by *Smith et al.* [2013] due to the inclusion of shot-to-shot variability. Unlike *Smith et al.* [2013], higher uncertainties attributed to these data reduce our confidence in any interpretation of significant lateral variations in basal properties. However, the overall interpretation remains unchanged, the acoustic impedance measurements are consistent with the basal shear calculations. Beneath Whillans Ice Stream, on the Siple Coast of West Antarctica, the presence of a deforming sediment layer [*Alley et al.*, 1987; *Blankenship et al.*, 1987] results in low basal resistance which allows high ice-flow velocities by basal slip. The acoustic impedance measurements here are consistent with this model being applicable to PIG, and as such indicate that basal conditions upstream will not inhibit further rapid retreat of PIG if the high-friction region directly upstream of the grounding line, currently restraining flow, is breached. Furthermore, there is no evidence of “sticky spots” which increase basal drag, as observed, for example, beneath Rutford [*Smith et al.*, 2015] or Kamb Ice Streams [*Anandakrishnan and Alley*, 1994].

Topographic features at the bed can reach heights of a few hundred meters over a few kilometers laterally and are comparable to those observed elsewhere beneath ice streams of West Antarctica [*Horgan et al.*, 2011]. The scale of these features is much greater than is normally attributed to drumlins [e.g., *Boulton*, 1987] or even mega-scale glacial lineations [*Clark*, 1993] and likely reflects deeper geological structure: features of this scale are unlikely to be formed purely by deforming sediment and there is likely to be a harder core over which sediment is draped, termed a “fixed core” when applied to drumlins [*Boulton*, 1987]. Although we are unable to determine the nature of this core, the discrete till layer on profile iSTARit between tributaries is consistent with a sediment layer overlying a more consolidated substrate. No sedimentary features are observed within the large basal topographic highs, indicating either massive homogeneous sedimentary sequences or a crystalline origin: Where the basal till layer is inferred to be absent (iSTARit, 3500 m, Figure 3a), higher acoustic impedance values indicate a well consolidated or lithified sediment, perhaps suggesting the former interpretation is more likely. Although features of this scale will oppose ice flow through form drag, the presence of dilated sediment at the bed will result in basal drag lower than that of an exposed hard bed [*Cuffey and Paterson*, 2010]. Similarly, invariant acoustic impedance measurements across a range of topographic features indicate that water pressures are not reduced locally, as might be expected, and as such stronger till does not always result over basal highs.

Although high-porosity subglacial till provides a readily deformable bed, and as such facilitates sliding, small changes in porosity can have a large influence on the degree of lubrication provided by the bed [*Tulaczyk et al.*, 2000b]. Both the Kamb and Whillans Ice Streams have shown significant reduction in flow rate and subsequent ice stream thickening [*Engelhardt and Kamb*, 2013; *Joughin et al.*, 2005] which has been attributed to changes at the bed [*Anandakrishnan and Alley*, 1997; *Winberry et al.*, 2014]. As such, minor reorganization of the stress regime or hydrological potential gradient beneath PIG, with subsequent effective pressure changes at the bed resulting from water pressure variation, may alter the effectiveness of the till to facilitate flow. However, the abundant supply and widespread distribution of sediments imply that the existing basal conditions will likely persist until a significant external forcing or internal reorganization takes place, perhaps as a result of retreat beyond the high-friction region upstream of the grounding line.

## 5. Conclusions

Seismic reflection profiles were collected across the main trunk and tributaries of Pine Island Glacier to constrain bed properties. Newly acquired profiles, combined with existing data, have been used to derive the calibrated reflection coefficient of the bed from the relative strength of the primary and multiple bed returns. This has been used to determine the acoustic impedance of the bed material which, combined with the seismic images, can be used to infer basal material and conditions. Variance in the results has been constrained by utilizing all available bed-multiple arrivals, along with uncertainties in all measured and assumed parameters.

Seismic profiles indicate older sedimentary deposits, providing sufficient material to maintain a widespread till layer at the ice base, despite considerable topographic variation. Combined with seismic reflection images, the measured acoustic impedance values indicate relatively uniform bed conditions beneath the main trunk and tributaries, with a widespread reworked sediment layer measured at up to 10 m thick in places with a dilated sediment lid of minimum thickness  $1.5 \pm 0.4$  m. Both radar and seismic surveys indicate considerable basal topography; seismic observations indicate that sediment is draped over these features. Beneath the intertributary ice, a discrete till layer of  $7 \pm 3$  m thickness is observed, of lower porosity than beneath the

fast-flowing tributaries. These combined results point to a highly mobile sediment body at the base of the ice with an abundant supply. We recognize that other interpretations of these data are feasible, although we believe the models presented here represent the most likely scenario and have taken care not to overinterpret variation in the observations. Subsequent targeted seismic amplitude-versus-angle or drilling campaigns would allow more definitive interpretations to be reached and a number of our assumptions to be tested.

Sediments of high porosity, as inferred here, provide a weak, readily deformable substrate which reduces basal drag and facilitates fast ice flow. This result is consistent with the results of the inversion of satellite data for shear stress at the bed. Both Joughin *et al.* [2009] and Arthern *et al.* [2015] infer relatively low shear stress values at the locations of all the seismic profiles with the exception of the site on slow-moving ice between two tributaries. The uniform bed conditions and nonuniform response of the individual tributaries discount any direct control by the basal material on the response of the individual tributaries to ice shelf thinning and grounding line retreat.

These measurements, in combination with detailed bed topography and digital elevation models of the surface, will allow detailed modeling of the subglacial regime to help better understand the hydrological system beneath the tributaries and the contribution this may make to the response of PIG to grounding line retreat.

# Acknowledgments

This work was supported by funding from the UK Natural Environment Research Council's iSTAR Programme, NERC grant NE/J005754/1 and from NERC grant NE/B502287/1. All fieldwork was supported by staff at the British Antarctic Survey's Rothera Research Station and members of the iSTAR Traverse. In particular, we thank Alex Taylor, James Wake, Tim Gee, Jonny Yates, Mark Baird, Julian Scott, Rob Smith, Roger Stilwell, Feargal Buckley, and Chris Griffiths for help with data acquisition. Data are available from the NERC Polar Data Centre ([www.bas.ac.uk/data/uk-pdc/](http://www.bas.ac.uk/data/uk-pdc/)). This manuscript was greatly improved with constructive comments from Hugh Horgan, one anonymous reviewer, and the Associate Editor, Olga Sergienko.

# References

- Alley, R. B., D. D. Blankenship, C. R. Bentley, and S. T. Rooney (1987), Till beneath ice stream-B 3. Till deformation—Evidence and implications, *J. Geophys. Res.*, *92*(B9), 8921–8929, doi:10.1029/JB092ib09p08921.
- Alley, R. B., S. Anandakrishnan, K. Christianson, H. J. Horgan, A. Muto, B. R. Parizek, D. Pollard, and R. T. Walker (2015), Oceanic forcing of ice-sheet retreat: West Antarctica and more, *Annu. Rev. Earth Planet. Sci.*, *43*, 207–231, doi:10.1146/annurev-earth-060614-105344.
- Anandakrishnan, S., and R. B. Alley (1994), Ice stream C, Antarctica, sticky spots detected by microearthquake monitoring, *Ann. Glaciol.*, *20*, 183–186.
- Anandakrishnan, S., and R. B. Alley (1997), Stagnation of ice stream C, West Antarctica by water piracy, *Geophys. Res. Lett.*, *24*, 265–268, doi:10.1029/96GL04016.
- Arthern, R. J., R. C. A. Hindmarsh, and C. R. Williams (2015), Flow speed within the Antarctic ice sheet and its controls inferred from satellite observations, *J. Geophys. Res. Earth Surf.*, *120*, 1171–1188, doi:10.1002/2014JF003239.
- Atre, S., and C. R. Bentley (1993), Laterally varying basal conditions beneath ice streams B and C, West Antarctica, *J. Glaciol.*, *39*(133), 507–514.
- Bentley, C. R., and H. Kohlen (1976), Seismic refraction measurements of internal friction in Antarctic ice, *J. Geophys. Res.*, *81*(8), 1519–1526, doi:10.1029/JB081i008p01519.
- Bindschadler, R. A. (2002), History of lower Pine Island Glacier, West Antarctica, from Landsat imagery, *J. Glaciol.*, *48*(163), 536–544.
- Bingham, R. G., D. Davies, E. C. King, S. L. Cornford, D. G. Vaughan, J. D. Rydt, and A. M. Smith (2014), The nature and dynamics of the bed beneath Pine Island Glacier, Antarctica, paper presented at WAIS meeting, Julian, Calif.
- Blankenship, D. D., C. R. Bentley, S. T. Rooney, and R. B. Alley (1986), Seismic measurements reveal a saturated porous layer beneath an active Antarctic ice stream, *Nature*, *322*(6074), 54–57, doi:10.1038/322054a0.
- Blankenship, D. D., C. R. Bentley, S. T. Rooney, and R. B. Alley (1987), Till beneath ice stream-B 1. Properties derived from seismic travel-times, *J. Geophys. Res.*, *92*(B9), 8903–8911, doi:10.1029/JB092ib09p08903.
- Booth, A. D., R. A. Clark, B. Kulesa, T. Murray, J. Carter, S. Doyle, and A. Hubbard (2012), Thin-layer effects in glaciological seismic amplitude-versus-angle (AVA) analysis: Implications for characterising a subglacial till unit, Russell Glacier, West Greenland, *Cryosphere*, *6*(4), 909–922, doi:10.5194/tc-6-909-2012.
- Boulton, G. S. (1987), A theory of drumlin formation by subglacial sediment deformation, in *Drumlin Symposium*, edited by J. Menzies and J. Rose, pp. 25–80, Balkema, Rotterdam, Netherlands.
- Brown, N. E., B. Hallet, and D. B. Booth (1987), Rapid soft bed sliding of the Puget Glacial Lobe, *J. Geophys. Res.*, *92*(B9), 8985–8997, doi:10.1029/JB092ib09p08985.
- Clark, C. D. (1993), Mega-scale glacial lineations and cross-cutting ice-flow landforms, *Earth Surf. Process. Landf.*, *18*(1), 1–29, doi:10.1002/esp.3290180102.
- Cuffey, K. M., and W. S. B. Paterson (2010), *The Physics of Glaciers*, Acad. Press, New York.
- Engelhardt, H., and B. Kamb (1998), Basal sliding of ice stream B, West Antarctica, *J. Glaciol.*, *44*(147), 223–230.
- Engelhardt, H., and B. Kamb (2013), Kamb ice stream flow history and surge potential, *Ann. Glaciol.*, *54*(63), 287–298, doi:10.3189/2013AoG63A535.
- Fretwell, P., *et al.* (2013), Bedmap2: Improved ice bed, surface and thickness datasets for Antarctica, *Cryosphere*, *7*(1), 375–393, doi:10.5194/tc-7-375-2013.
- Holland, C. W., and S. Anandakrishnan (2009), Subglacial seismic reflection strategies when source amplitude and medium attenuation are poorly known, *J. Glaciol.*, *55*(193), 931–937.
- Horgan, H. J., S. Anandakrishnan, R. B. Alley, P. G. Burkett, and L. E. Peters (2011), Englacial seismic reflectivity: Imaging crystal-orientation fabric in West Antarctica, *J. Glaciol.*, *57*(204), 639–650.
- Horgan, H. J., K. Christianson, R. W. Jacobel, S. Anandakrishnan, and R. B. Alley (2013), Sediment deposition at the modern grounding zone of Whillans Ice Stream, West Antarctica, *Geophys. Res. Lett.*, *40*, 3934–3939, doi:10.1002/grl.50712.
- Jenkins, A., P. Dutrieux, S. S. Jacobs, S. D. McPhail, J. R. Perrett, A. T. Webb, and D. White (2010), Observations beneath Pine Island Glacier in West Antarctica and implications for its retreat, *Nat. Geosci.*, *3*(7), 468–472, doi:10.1038/ngeo890.
- Joughin, I., *et al.* (2005), Continued deceleration of Whillans Ice Stream, West Antarctica, *Geophys. Res. Lett.*, *32*, L22501, doi:10.1029/2005GL024319.
- Joughin, I., S. Tulaczyk, J. L. Bamber, D. Blankenship, J. W. Holt, T. Scambos, and D. G. Vaughan (2009), Basal conditions for Pine Island and Thwaites Glaciers, West Antarctica, determined using satellite and airborne data, *J. Glaciol.*, *55*(190), 245–257, doi:10.3189/002214309788608705.



- Kamb, B. (2001), Basal zone of the West Antarctic ice streams and its role in lubrication of their rapid motion, in *The West Antarctic Ice Sheet: Behavior and Environment*, edited by R. B. Alley and R. A. Bindschadler, pp. 157–199, AGU, Washington, D. C., doi:10.1029/AR077p0157.
- Kirchner, J. F., and C. R. Bentley (1990), RIGGS III: Seismic short-refraction studies using an analytical curve-fitting technique, *Ant. Res. Series*, 42, 109–126.
- Lowe, A. L., and J. B. Anderson (2003), Evidence for abundant subglacial meltwater beneath the paleo-ice sheet in Pine Island Bay, Antarctica, *J. Glaciol.*, 49, 125–138, doi:10.3189/172756503781830971.
- Luthra, T., S. Anandakrishnan, J. P. Winberry, R. B. Alley, and N. Holschuh (2016), Basal characteristics of the main sticky spot on the ice plain of Whillans Ice Stream, Antarctica, *Ear. Planet. Sci. Lett.*, 440, 12–19, doi:10.1016/j.epsl.2016.01.035.
- McMillan, M., A. Shepherd, A. Sundal, K. Briggs, A. Muir, A. Ridout, A. Hogg, and D. Wingham (2014), Increased ice losses from Antarctica detected by CryoSat-2, *Geophys. Res. Lett.*, 41, 3899–3905, doi:10.1002/2014GL060111.
- Medley, B., et al. (2014), Constraining the recent mass balance of Pine Island and Thwaites glaciers, West Antarctica, with airborne observations of snow accumulation, *Cryosphere*, 8(4), 1375–1392, doi:10.5194/tc-8-1375-2014.
- Muto, A., L. E. Peters, K. Gohl, I. Sasgen, R. B. Alley, S. Anandakrishnan, and K. L. Riverman (2016), Subglacial bathymetry and sediment distribution beneath Pine Island Glacier ice shelf modeled using aerogravity and in situ geophysical data: New results, *Ear. Planet. Sci. Lett.*, 433, 63–75.
- Nias, I. J., S. L. Cornford, and A. J. Payne (2016), Contrasting the modelled sensitivity of the Amundsen Sea Embayment ice streams, *J. Glaciol.*, 62(233), 552–562, doi:10.1017/jog.2016.40.
- Nitsche, F. O., K. Gohl, R. D. Larer, C. D. Hillenbrand, G. Kuhn, J. A. Smith, S. Jacobs, J. B. Anderson, and M. Jakobsson (2013), Paleo ice flow and subglacial meltwater dynamics in Pine Island Bay, West Antarctica, *Cryosphere*, 7(1), 249–262, doi:10.5194/tc-7-249-2013.
- Peters, L. E., S. Anandakrishnan, R. B. Alley, J. P. Winberry, D. E. Voigt, A. M. Smith, and D. L. Morse (2006), Subglacial sediments as a control on the onset and location of two Siple Coast ice streams, West Antarctica, *J. Geophys. Res.*, 111, B01302, doi:10.1029/2005JB003766.
- Peters, L. E., S. Anandakrishnan, R. B. Alley, and D. E. Voigt (2012), Seismic attenuation in glacial ice: A proxy for englacial temperature, *J. Geophys. Res.*, 117, F02008, doi:10.1029/2011JF002201.
- Pollard, D., and R. M. DeConto (2009), Modelling West Antarctic ice sheet growth and collapse through the past five million years, *Nature*, 458(7236), 329–333, doi:10.1038/nature07809.
- Rignot, E., J. L. Bamber, M. R. Van Den Broeke, C. Davis, Y. H. Li, W. J. Van De Berg, and E. Van Meijgaard (2008), Recent Antarctic ice mass loss from radar interferometry and regional climate modelling, *Nat. Geosci.*, 1(2), 106–110, doi:10.1038/ngeo102.
- Rignot, E., J. Mouginot, and B. Scheuchl (2011a), *MEASURES Antarctic Grounding Line From Differential Satellite Radar Interferometry*, NASA EOSDIS Distributed Active Archive Center at NSIDC, Boulder, Colo., Accessed on 17 June 2016.
- Rignot, E., I. Velicogna, M. R. van den Broeke, A. Monaghan, and J. Lenaerts (2011b), Acceleration of the contribution of the Greenland and Antarctic ice sheets to sea level rise, *Geophys. Res. Lett.*, 38, L05503, doi:10.1029/2011GL046583.
- Rippin, D. M., D. G. Vaughan, and H. F. J. Corr (2011), The basal roughness of Pine Island Glacier, West Antarctica, *J. Glaciol.*, 57(201), 67–76, doi:10.3189/002214311795306574.
- Ritz, C., T. L. Edwards, G. Durand, A. J. Payne, V. Peyaud, and R. C. Hindmarsh (2015), Potential sea-level rise from Antarctic ice-sheet instability constrained by observations, *Nature*, 528(7580), 115–118, doi:10.1038/nature16147.
- Roethlisberger, H. (1972), *Seismic Exploration in Cold Regions*, Rep. Monogr. II A2a, 153 pp., U.S. Army Cold Reg. Res. and Eng. Lab., Hanover, N. H.
- Rooney, S. T., D. D. Blankenship, R. B. Alley, and C. R. Bentley (1987), Till beneath ice stream-B2. Structure and Continuity, *J. Geophys. Res.*, 92(B9), 8913–8920, doi:10.1029/JB092iB09p08913.
- Scambos, T. A., T. M. Haran, M. A. Fahnestock, T. H. Painter, and J. Bohlander (2007), MODIS-based Mosaic of Antarctica (MOA) data sets: Continent-wide surface morphology and snow grain size, *Remote Sens. Environ.*, 111(2–3), 242–257, doi:10.1016/j.rse.2006.12.020.
- Scott, J. B. T., A. M. Smith, R. G. Bingham, and D. G. Vaughan (2010), Crevasses triggered on Pine Island Glacier, West Antarctica, by drilling through an exceptional melt layer, *Ann. Glaciol.*, 51(55), 65–70, doi:10.3189/172756410791392763.
- Shepherd, A., et al. (2012), A reconciled estimate of ice-sheet mass balance, *Science*, 338(6111), 1183–1189, doi:10.1126/science.1228102.
- Smith, A. M. (1997a), Basal conditions on Rutford Ice Stream, West Antarctica, from seismic observations, *J. Geophys. Res.*, 102, 543–552, doi:10.1029/96JB02933.
- Smith, A. M. (1997b), Variations in basal conditions on Rutford Ice Stream, West Antarctica, *J. Glaciol.*, 43(144), 245–255.
- Smith, A. M. (2007), Seismic reflection and subglacial conditions, *J. Env. Eng. Geophys.*, 12(1), 3–13.
- Smith, A. M., T. A. Jordan, F. Ferraccioli, and R. G. Bingham (2013), Influence of subglacial conditions on ice stream dynamics: Seismic and potential field data from Pine Island Glacier, West Antarctica, *J. Geophys. Res.-Solid Earth*, 118(4), 1471–1482, doi:10.1029/2012JB009582.
- Smith, E. C., A. M. Smith, R. S. White, A. M. Brisbourne, and H. D. Pritchard (2015), Mapping the ice-bed interface characteristics of Rutford Ice Stream, West Antarctica, using microseismicity, *J. Geophys. Res.-Earth Surf.*, 120, 1881–1894, doi:10.1002/2015JF003587.
- Stenoien, M. D., and C. R. Bentley (2000), Pine Island Glacier, Antarctica: A study of the catchment using interferometric synthetic aperture radar measurements and radar altimetry, *J. Geophys. Res.*, 105(B9), 21,761–21,779, doi:10.1029/2000JB900151.
- Tulaczyk, S., B. Kamb, R. P. Scherer, and H. F. Engelhardt (1998), Sedimentary processes at the base of a West Antarctic ice stream: Constraints from textural and compositional properties of subglacial debris, *J. Sedim. Res.*, 68(3), 487–496.
- Tulaczyk, S., W. B. Kamb, and H. F. Engelhardt (2000a), Basal mechanics of ice stream B, West Antarctica 1. Till mechanics, *J. Geophys. Res.*, 105(B1), 463–481, doi:10.1029/1999JB900329.
- Tulaczyk, S., W. B. Kamb, and H. F. Engelhardt (2000b), Basal mechanics of ice stream B, West Antarctica: 2. Undrained plastic bed model, *J. Geophys. Res.*, 105(B1), 483–494, doi:10.1029/1999JB900328.
- Vaughan, D. G., A. M. Smith, P. C. Nath, and E. Le Meur (2003), Acoustic impedance and basal shear stress beneath four Antarctic ice streams, *Ann. Glaciol.*, 36, 225–232.
- Voigt, D., L. E. Peters, and S. Anandakrishnan (2013), ‘Georods’: The development of a four-element geophone for improved seismic imaging of glaciers and ice sheets, *Ann. Glaciol.*, 54(64), 142–148.
- Winberry, J. P., S. Anandakrishnan, R. B. Alley, D. A. Wiens, and M. J. Pratt (2014), Tidal pacing, skipped slips and the slowdown of Whillans Ice Stream, Antarctica, *J. Glaciol.*, 60(222), 795–807, doi:10.3189/2014JG14J038.
- Wingham, D. J., D. W. Wallis, and A. Shepherd (2009), Spatial and temporal evolution of Pine Island Glacier thinning, 1995–2006, *Geophys. Res. Lett.*, 36, L17501, doi:10.1029/2009GL039126.